Tumor-Penetrating Nanotherapeutics Loading a Near-Infrared Probe Inhibit Growth and Metastasis of Breast Cancer

Xinyu He, Xiaoyue Bao, Haiqiang Cao, Zhiwen Zhang, Qi Yin, Wangwen Gu, Lingli Chen, Haijun Yu, and Yaping Li**

The tumor growth and metastasis is the leading reason for the high mortality of breast cancer. Herein, it is first reported a deep tumor-penetrating photothermal nanotherapeutics loading a near-infrared (NIR) probe for potential photothermal therapy (PTT) of tumor growth and metastasis of breast cancer. The NIR probe of 1,1-dioctadecyl-3,3,3,3-tetramethylindotricarbocyanine iodide (DiR), a lipophilicfluorescent carbocyanine dye with strong light-absorbing capability, is entrapped into the photothermal nanotherapeutics for PTT application. The DiR-loaded photothermal nanotherapeutics (DPN) is homogeneous nanometer-sized particles with the mean diameter of 24.5 ± 4.1 nm. Upon 808 nm laser irradiation, DPN presents superior production of thermal energy than free DiR both in vitro and in vivo. The cell proliferation and migration activities of metastatic 4T1 breast cancer cells are obviously inhibited by DPN in combination with NIR irradiation. Moreover, DPN can induce a higher accumulation in tumor and penetrate into the deep interior of tumor tissues. The in vivo PTT measurements indicate that the growth and metastasis of breast cancer are entirely inhibited by a single treatment of DPN with NIR irradiation. Therefore, the deep tumor-penetrating DPN can provide a promising strategy for PTT of tumor progression and metastasis of breast cancer.

1. Introduction

Breast cancer is the second leading cause of cancer-related mortality in females worldwide.[1,2] The disease can be treated when diagnosed early, but became largely incurable and fatal once they metastasize to distant organs at advanced stages.[1,3,4] In clinic, the metastasis is responsible for over 90% of breast cancer-related death. Despite the advances in new therapeutic agents, new combinational regimens and targeted therapies, the patients with metastatic breast cancer have a limited survival time of 18–24 months and the five-year survival rate is only about 20%.[1,5,6] To date, few patients with metastatic cancer can be cured by surgical intervention or other treatment modalities.[3,6] As a result, it is highly desirable to find new strategies for effective treatment of tumor growth and metastasis of breast cancer.

Recently, photothermal therapy (PTT), which employs the near-infrared (NIR) laser (650–1100 nm) photoabsorbers to generate heat from light absorption for thermal ablation of cancer cells,[7,8] has been identified as an encouraging and noninvasive treatment modality of cancer,[7,9,10] but its applications on inhibiting cancer metastasis are seldom reported. Up to now, a variety of organic/inorganic nanomaterials, such as polypyrrole nanoparticles (NPs),[11] metal NPs,[12] semiconductors NPs,[13] and carbon-based nanostructures (carbon nanotubes or graphenes),[9,14] have been extensively explored as photothermal nanotherapeutics of PTT. However, these nanomaterials are usually nonbiodegradable, immunogenic, and have potential long-term toxicity, which significantly limited their clinical applications.[15] Therefore, it is worth raising concerns regarding efficient photothermal nanotherapeutics for potential application in PTT.

Alternatively, a great interest has been devoted to NIR fluorescence dyes and their nanoassemblies for PTT applications.[16,17] Typically, 1,1-dioctadecyl-3,3,3,3-tetramethylindotricarbocyanine iodide (DiR) is a lipophilic NIR fluorescent dye with strong light-absorbing capability and negligible cytotoxicity at concentrations suitable for in vivo imaging.[18,19] Moreover, DiR has a maximal emission wavelength of 782 nm with high fluorescence quantum yield, which make it a particularly promising candidate for PTT application.[19] However, the lipophilic DiR is prone to aggregate in water, thereby leading to the loss of fluorescence quantum yield and depression of fluorescent intensity. To avoid these drawbacks, DiR can be incorporated into nanoparticles to achieve the high fluorescent intensity and photostability.[20] Up to now, DiR alone or in combination with polymeric nanoparticles has been used for in vivo optical imaging and cell tracking.[19,21] However, as a strong

X. He, X. Bao, H. Cao, Dr. Z. Zhang, Dr. Q. Yin, W. Gu, L. Chen, Dr. H. Yu, Prof. Y. Li
State key Laboratory of Drug Research & Center of Pharmaceutics
Shanghai Institute of Materia Medica
Chinese Academy of Sciences
Shanghai 201203, China
E-mail: zwzhang0125@simm.ac.cn; ypli@simm.ac.cn

DOI: 10.1002/adfm.201500772

NIR light-absorber, its potential photothermal therapeutic effects have not been explored yet.

With respect to the extremely complicated and abnormal tumor microenvironments, the deep tumor-penetration of photothermal nanotherapeutics can be an essential prerequisite for effective PTT. It was reported that the poor penetration of nanoparticles in solid tumors was a main cause for its inadequate therapeutic efficacy.[22,23] Nanotherapeutics can passively accumulate into the tumor site owing to the enhanced permeability and retention (EPR) effects,[24,25] but they distribute only in the perivascular space of tumor areas, and their deeper penetration into the tumor tissues is significantly impeded due to the physiological barriers of tumor.[22,26,27] Fortunately, it is found that the smaller-sized nanoparticles showed superior tumor penetration capability,[28] for example, among different polymeric micelles with diameters ranging from 30 to 100 nm, only the 30 nm micelles could penetrate into the poorly permeable tumors and present an antitumor effect.[29] Thereby, it can be reasonable to control the particle size of nanotherapeutics to achieve a deep tumor-penetrating effect to enhance the PTT efficacy.

Herein, we put forward a novel deep tumor-penetrating DiR-loaded photothermal nanotherapeutics (DPN) for PTT of tumor growth and metastasis of breast cancer. The lipophilic DiR and amphiphilic polymer of poly(ethylene glycol)-*block*-poly(2-diisopropylmethacrylate) (PEG-*b*-PDPA) were assembled into nanometer-sized DPN with the mean diameter within 20–30 nm. We predicted that DPN could penetrate into the deep of tumor tissues and be changed into nano-firebombs upon NIR irradiation for photothermal ablation of cancer cells (**Scheme 1**).

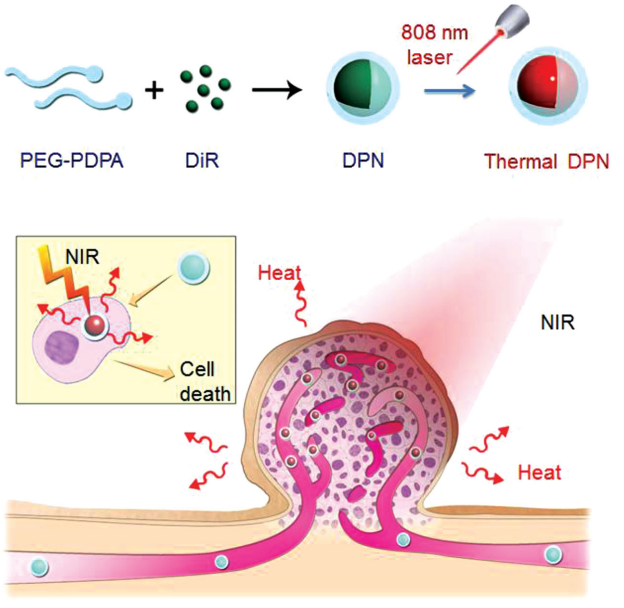

Scheme 1. DiR-loaded photothermal nanotherapeutics (DPN) for PTT of breast cancer. The DiR and PEG-*b*-PDPA could be assembled into photothermal nanotherapeutics to improve the thermal energy production under NIR laser irradiation. Moreover, DPN could specifically accumulate in tumor and penetrate into the deep inner side of tumor. Upon 808 nm laser irradiation, DPN could be changed into nano-firebombs for effective PTT of tumor growth and metastasis of breast cancer.

The fluorescent intensity and heat-generating capability of DiR were greatly enhanced after its encapsulation into DPN. The high accessibility of DPN in tumor site was investigated by NIR fluorescence imaging, and the deep tumor penetration was verified by photoacoustic imaging. The PTT abilities of DPN on cell proliferation and migration were evaluated in metastatic 4T1 breast cancer cells. In particular, the inhibitory effects of DPN on tumor progression and lung metastasis of breast cancer were validated in 4T1-luc induced metastatic breast cancer models.

2. Results and Discussion

2.1. Characterization of DPN

Herein, the lipophilic DiR was assembled with amphiphilic polymer of PEG-*b*-PDPA to form the nanoscaled DPN to improve the fluorescence intensity and heat-generating capability during NIR irradiation (**Figure 1**A). The methoxy poly(ethylene glycol) (mPEG)-*b*-PDPA copolymer was synthesized by the atom-transfer radical polymerization (ATRP) method. It was determined that there were about ten units of diisopropylmethacrylate (DPA) monomers linked to the mPEG molecules. The details of the synthesis procedure and NMR spectroscopic characterization were described in the Supporting Information (Figures S1–S3, Supporting Information). To determine the formation of photothermal nanotherapeutics, the morphology of DPN was determined by transmission electron microscopy (TEM) measurements, which showed that DPN was homogenous spherical nanoparticles with the mean diameter of 24.5 ± 4.1 nm (Figure 1B). It was reported that the nanoparticles with smaller size could facilitate their deeper penetration in tumor tissues.[26,28,29] Accordingly, the small size of DPN could be beneficial for its deep penetration in tumor tissues to enhance the PTT efficacy.

Then, the enhancement of DPN on the fluorescence intensity and heat-generating capability was further determined. Although DiR is an ideal candidate for in vivo PTT upon NIR irradiation, DiR is almost self-quenched in water, which could reduce the photothermal effects and the therapeutic efficacy of PTT (Figure 1C–E). The measured results showed great difference in the fluorescence intensity and photothermal effects were evidently detected between free DiR and DPN. The fluorescence intensity of free DiR at 780 nm was extremely low in water with excitation at 745 nm, but greatly increased after its encapsulation into DPN (Figure 1C). Meanwhile, the temperature of free DiR in water was only slightly increased to 39.8 ± 0.8 °C after their exposure to the 808 nm laser at 2.5 W cm^{-2} for 5 min. However, when DiR was encapsulated into DPN, the temperature was significantly increased to 48.8 ± 1.0 °C during NIR irradiation (Figure 1E). Thereby, DPN could induce a higher production of thermal energy than free DiR, which was also depicted in the infrared thermographic images (Figure 1D). The significant enhancement of temperature by DPN could lead to the irreversible damages to cancer cells.[17] These findings clearly verified the superior efficiency of DPN over free DiR on enhancing the photothermal effects, which demonstrated its great potential for effective PTT.

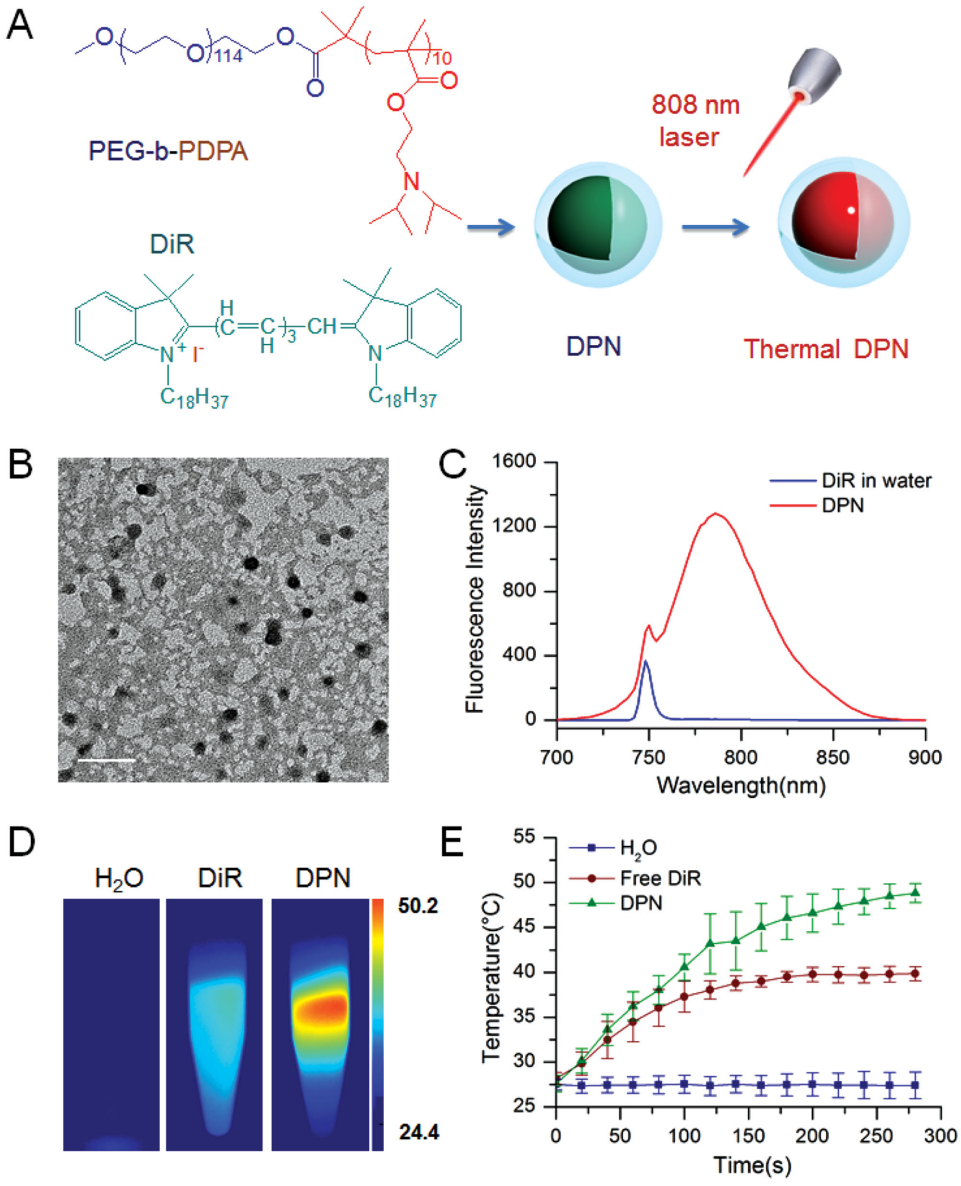

Figure 1. Preparation and characterization of DPN. A) Preparation of DPN; B) typical TEM image of DPN, scale bar = 100 nm; C) fluorescence spectra of free DiR in water and DPN (excitation/emission 745/780 nm). D) Infrared thermalgraphic images of H_2O, free DiR, and DPN at 5 min of laser irradiation; E) temperature elevation profile of H_2O, free DiR (0.2 mg mL^{-1}), and DPN (containing 200 μg mL^{-1} DiR) as a function of irradiation time.

2.2. In Vitro PTT Effects of DPN on Cell Viability and Migration

To detect the in vitro PTT efficacy of DPN, we investigated the photothermal effects and temperature increments in 4T1 breast cancer cells upon NIR irradiation. Cells were pretreated with free DiR or DPN, and then irradiated with the 808 nm laser at a power density of 2.5 W cm^{-2}. The nontreated cells with NIR irradiation were performed as control. The temperature changes were recorded with an infrared thermal camera. The thermal signals of DPN-treated 4T1 cells was gradually increased to the maximum within 80 s, and then remained the steady state during the NIR irradiation (**Figure 2**). Moreover, the temperature of DPN-treated cells dramatically rose up to 53.0 ± 2.2 °C, whereas that of free DiR treated cells was only increased to 38.8 ± 2.5 °C from the room temperature (Figure 2). By contrast, the temperature of nontreated cells was hardly changed during the NIR irradiation. Thereby, DPN was more efficient in producing NIR-dependent temperature increase than free DiR in 4T1 cells, which could enable the photothermal ablation of cancer cells.

Then, the photothermal cytotoxicity of DPN in metastatic breast cancer 4T1 cells was determined by LIVE/DEADViability/Cytotoxicity Kit to evaluate the PTT effects on cell viability. In living cells, the calcein M of the kit could be internalized and converted into fluorescent calcein, thereby producing an intense green fluorescence. By contrast, the EthD-1 in the kit could only enter the dead cells with damaged membrane, and then present a bright red fluorescence upon binding

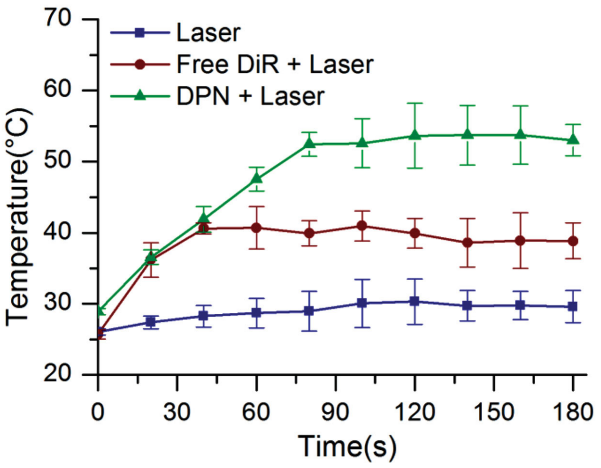

Figure 2. The temperature increase profile of DPN in 4T1 cells as a function of irradiation time. Cells were previously treated with free DiR or DPN and then exposed to NIR irradiation. Cells treated with laser alone were performed as control.

to nucleic acid. Cells were pretreated with free DiR or DPN, and then exposed to the 808 nm laser at a power density of 2.5 W cm^{-2}. By contrast, cells in free DiR and DPN groups without NIR irradiation were performed as control (Figure S4, Supporting Information). A large amount of green fluorescence signals were obviously observed in nontreated cells, DiR and DPN treated cells without NIR irradiation, and nontreated cells with NIR irradiation alone (**Figure 3** and Figure S4, Supporting Information). These experimental results suggested the negligible toxicity of free DiR and DPN alone, and even NIR irradiation alone in metastatic 4T1 cells. However,

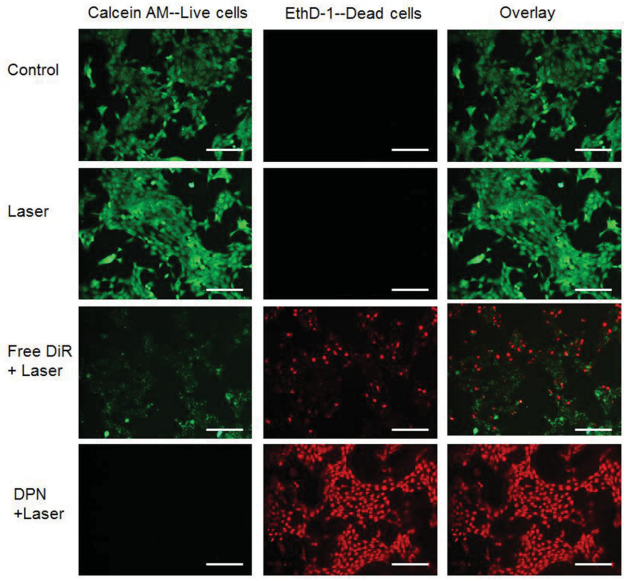

Figure 3. Photothermal cytotoxicity of DPN in 4T1 cells. Live/dead viability assay were performed for 4T1 cells with or without NIR irradiation under different treatments. The live cells could be stained with calcein AM (green), whereas the dead cells were labeled with EthD-1. Scale bar = 100 μm.

in free DiR+laser treated group, a few red fluorescence spots and plenty of green fluorescence signals were detected. Moreover, in DPN+laser treated group, only red fluorescence signals were largely observed (Figure 3). These observations indicated that a limited quantity of cells were dead in the free DiR with laser treatment, but almost all cells were scalded to death in DPN with NIR irradiation. Thereby, DPN could induce higher photothermal cytotoxicity than free DiR in cancer cells upon NIR irradiation.

Moreover, the PTT effects of DPN on cell migration activities of 4T1 cells were evaluated, in which the irradiation time was carefully controlled not to induce obvious cell death. To avoid the interference of cell death on cell migration activities, the cell viability was detected by the LIVE/DEADViability/Cytotoxicity Kit. At a power density of 2.5 W cm^{-2}, cells were exposed to the NIR laser for only 1 min and no obvious damages were detectable in DPN and free DiR treated groups (**Figure 4**A). Then, the cell migration activities were measured by the transwell migration assay.[30] The measured results indicated that PTT with free DiR or DPN could achieve distinct inhibitory effects on cell migration of metastatic 4T1 cells (Figure 4B). Compared with the negative control, the cell migration in NIR laser treated group was slightly reduced. However, in free DiR and DPN treated group, almost no migrated cells were detected. Compared with the negative control, the percentage of migrated cells was obviously reduced to 1.9% for free DiR with laser group and 1.8% for DPN with laser group (Figure 4C). In addition, the cell migration was hardly inhibited in free DiR and DPN group without NIR irradiation (Figure S5, Supporting Information). These results indicated that PTT was capable of suppressing cell migration ability before inducing cell death. Thereby, the in vitro PTT measurements clearly verified the effectiveness of DPN on inhibition of cell viability and migration activities, which could be potential for treating the progression and metastasis of cancer cells.

2.3. In Vivo Biodistribution and Penetration in Tumor Tissues

The high accessibility of DPN in tumor site is of great significance for effective PTT. As DiR was a common NIR probe for in vivo imaging, the in vivo biodistribution profiles of DPN and free DiR were monitored by detecting its fluorescence signals in tumor xenografts at different time points (**Figure 5**A). The captured images indicated that the fluorescence signals of DPN could be detected in tumor area at 0.5 h after injection, and then gradually increased with time. Moreover, the fluorescence signals of DPN were obviously higher than that of free DiR. At 1.0 h after the administration, the major organs and tumor were excised for NIR fluorescence imaging (Figure 5B). Particularly in tumor tissues, the fluorescence intensity from DPN was greatly improved 6.6 times over that from free DiR (Figure 5C). The nanotherapeutics with the particle size in the range of 20–200 nm can extravagate from blood circulation and retained in tumor tissue.[25] The significantly increased accumulation of DPN in tumor could result from the prolonged lifetime of DiR in blood circulation and the enhanced EPR effects due to the nanometric particle size.

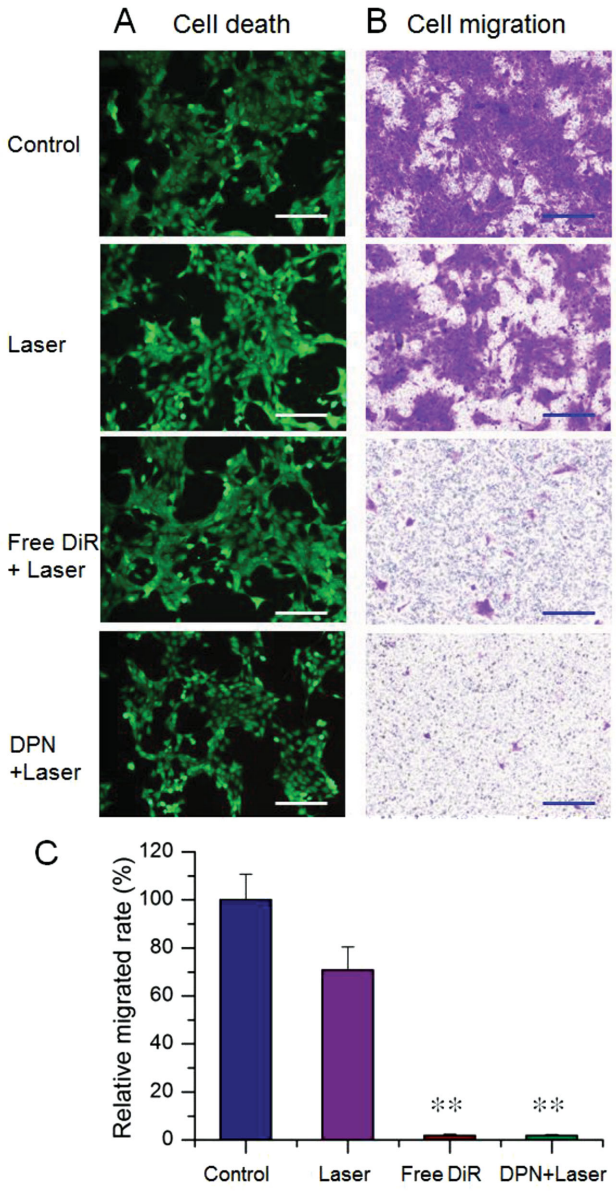

Figure 4. In vitro PTT abilities of DPN on inhibition of cell migration activities of 4T1 metastatic cells. Cell previously treated with DiR or DPN and irradiated under NIR laser at 2.5 W cm^{-2} for 1 min for transwell migration assay. A) Live/dead cell viability assay. B) Typical images of migrated cells across the membrane; C) quantification of inhibition on cell migration. Scale bar = 100 μm, $^{**}p < 0.01$.

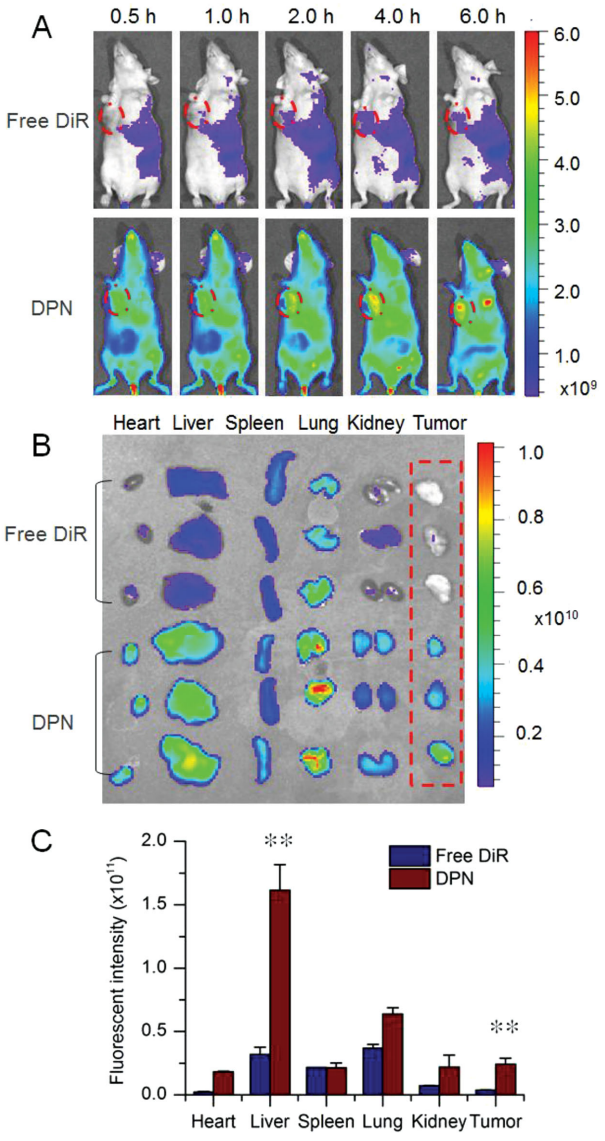

Figure 5. In vivo distribution of DPN in 4T1-luc cells induced metastatic breast cancer model. A) NIR fluorescence images of free DiR or DPN treated mice at different time points; B) NIR fluorescence images of major organs and tumor at 1 h after injection. C) Quantification of fluorescence intensity of each organ from DiR and DPN group, $^{**}p < 0.01$.

Then, the deep penetration of DPN in tumor was further verified by the multispectral optacoustic tomographic (MSOT) imaging system, which could provide a series of transverse sections from surface to depth of tumor tissue. It reported that the smaller-sized nanotherapeutics had superior efficacy on enhancement of tumor penetration.[28,29] The particle size of DPN was mainly in the range of 20–30 nm, which could be promising to penetrate into the deep interior of tumor tissues. The measured results indicated that DPN could distribute in the full extent of the tumor tissues in an uneven manner. The photoacoustic signals of DPN were gradually enhanced when the tumor was scanned from the surface to the interior (**Figure 6**). Moreover, DPN could be mainly distributed heterogeneously in the interior of the tumor. These observations indicated that DPN could penetrate into the deep inner side of the tumor, which could result from the newly developed blood vessels in tumor and the small particle size of DPN. Once DPN was penetrated into the deep of tumor tissue, it could generate high levels of thermal energy upon NIR irradiation and be changed into deep-penetrating nano-firebombs for photothermal ablation of cancer cells. Thereby, the high accessibility of DPN in tumor and its deep tumor penetrating capability could provide an essential prerequisite for effective PTT of cancer.

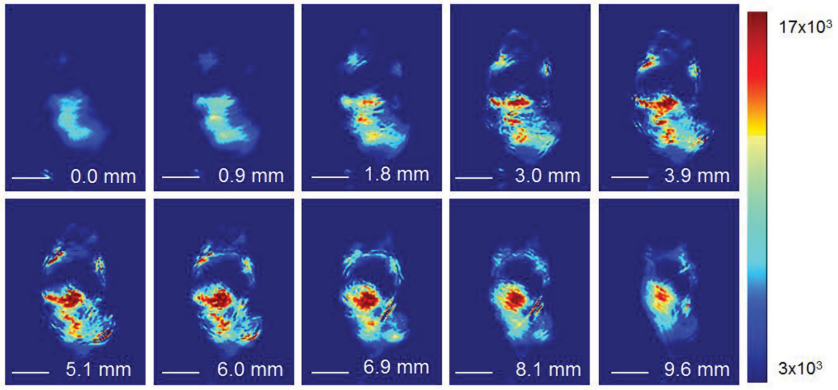

Figure 6. The photoacoustic signals images of DPN in tumor with the depth from 0 to 9.6 mm, scale bar = 3 mm. DPN was injected to tumor bearing mice via tail vein. At 1.0 h, tumor was excised and the distribution of DPN in tumor was measured by the multispectral optacoustic tomographic (MSOT) imaging system.

2.4. In Vivo Photothermal Imaging and PTT Effect on Growth and Metastasis of Breast Cancer

During photothermal treatment, the in vivo thermographic images were captured to record the temperature changes under NIR irradiation by 808 nm laser at a power density of 2.5 W cm^{-2}. The tumor bearing mice were, respectively, intravenously administered with saline, free DiR and DPN, and then irradiated with the NIR laser at 1.0 h after the injection. The captured images indicated that an obvious enhancement of tumor temperature was detected in both free DiR and DPN treated groups (**Figure 7**A). Within 5 min of NIR irradiation, the thermal signals of tumor rapidly increased over time and plateaued to the maximum. The maximal tumor temperature in free DiR+laser group was 47.1 ± 2.4 °C, which showed no significant difference from that of laser control (45.2 ± 1.1 °C). However, in DPN+laser treated group, the tumor temperature was obviously elevated to 54.3 ± 1.7 °C, which was much higher than that of free DiR+laser and laser groups (Figure 7B). The enhancement of tumor temperature could mainly attribute to the higher specific accumulation in tumor and the superior heat-generating capability of DPN over free DiR. Moreover, the maximal temperature of tumor in DPN treated group was far beyond the threshold needed to induce thermal ablation of cancer cells, which demonstrated great potential for PTT.

Then, the in vivo PTT effect of DPN on the growth and metastasis of breast cancer was measured in metastatic breast cancer model. Mice were randomly divided into four groups of negative control, laser, free DiR+laser, and DPN+laser. The photothermal treatments were performed at day 8 after inoculation. The representative images of tumor-bearing mice from each group were shown in **Figure 8**A at the end point of PTT treatment. The images indicated that tumors area was clearly observable in negative control, laser, and free DiR+laser group, but almost eliminated with necrotic scar left at the original tumor site (Figure 8A). In the tumor growth profiles, the tumor size of DPN+laser group shrank gradually to zero within the first 10 d after NIR irradiation, but re-emerged to about 150 mm^3 thereafter (Figure 8B). By contrast, compared with the negative control, a slight inhibition of tumor growth was detected in mice treated with laser alone or free DiR+laser. At the end point, the tumor volume of DPN+laser treated group was only 15.6% of laser alone and 20.2% of the free DiR+laser group (Figure 8C). The DPN+laser could result in 87.9% reduction of tumor growth, which was, respectively, 3.9-fold higher than that of laser irradiation alone and 2.2-folds higher than that of free DiR+laser group. In addition, the body weight was not significantly changed among these four groups during the treatment (Figure S6, Supporting Information). Thereby, DPN could effectively lessen tumor burden and inhibit tumor growth upon NIR laser irradiation.

Moreover, we evaluated the PTT effect of DPN on inhibiting the lung metastasis of breast cancer. To some extent, over 90% of breast cancer-related death in clinic was mainly caused by the metastasis of breast cancer.[1,6] Lung tissue was one of the most common organs that breast cancer tended to spread to.[31] Accordingly, it could be a high priority to inhibit the lung metastasis of breast cancer for successful

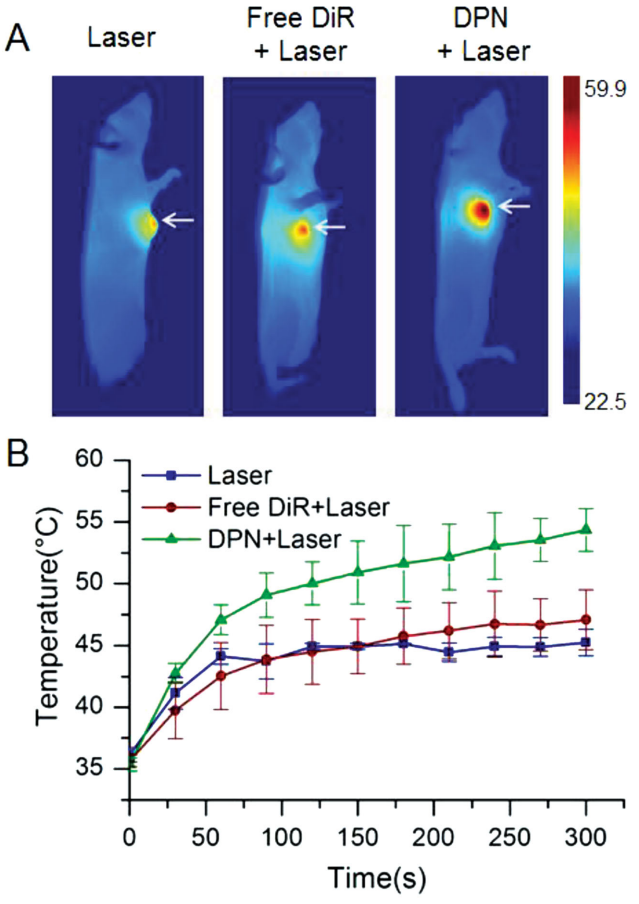

Figure 7. In vivo photothermal profiles of free DiR and DPN treated mice. A) Infrared thermographic images of tumor bearing mice after NIR irradiation (2.5 W cm^{-2} for 5 min). B) Temperature increase profiles of tumor tissues in mice treated with free DiR and DPN.

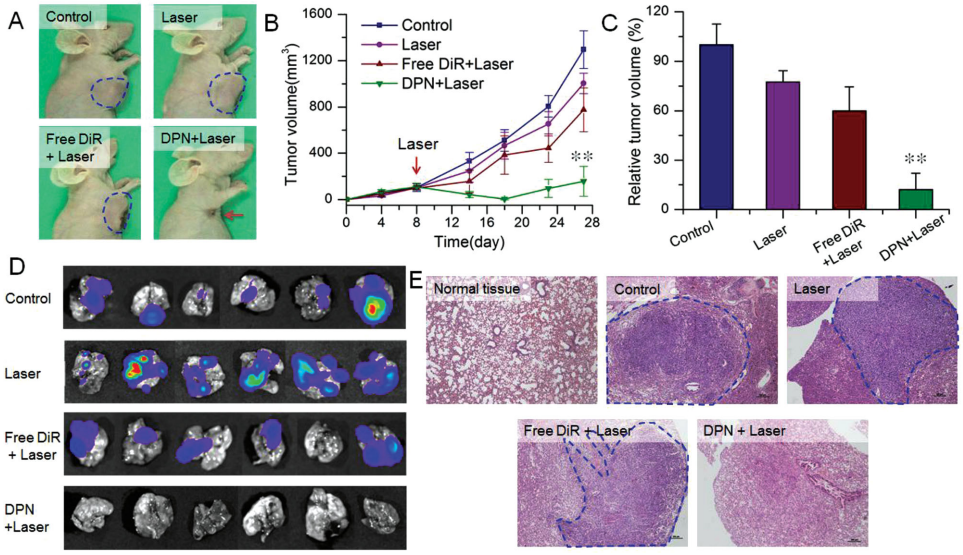

Figure 8. The in vivo therapeutic effect of DPN on tumor growth and metastasis of breast cancer. A) Typical images of tumor bearing mice at the end point from control, laser, free DiR+laser, and DPN+laser group; B) tumor growth profiles of each group, $^{**}p < 0.01$; C) the relative inhibition of tumor growth, $^{**}p < 0.01$; D) ex vivo bioluminescence images of lung tissues from each group under imaging system. E) Histological examinations of lung tissues from each group.

PTT. Herein, the 4T1-luc cells with stable expression of luciferase were used to develop the metastatic breast cancer model. The metastatic nodules in lungs could be readily detected by monitoring the bioluminescence signals from the luciferin–luciferase reactions.[30] The captured images showed plenty of bioluminescence signals in all the lung tissues of the negative control and laser groups, which verified the extensive occurrence of lung metastasis and the invalidity of laser irradiation alone on lung metastasis (Figure 8D). The bioluminescence signals were also detected in most lung tissues (5/6) of free DiR+laser group, but scarcely observed in those of DPN+laser group, which verified the superior therapeutic efficacy of DPN on inhibiting the lung metastasis. Moreover, the histological examinations of the lung tissue also confirmed that large area of metastasis nodules was obviously observed in control, laser, and free DiR+laser group, but no metastatic foci were detected in DPN+laser group (Figure 8E). These experimental results indicated that the lung metastasis of breast cancer could be effectively inhibited by DPN combined with NIR irradiation. Thereby, the DPN+laser treatment could result in a significant inhibition of growth and metastasis of breast cancer, which was undoubtedly more effective than that of free DiR+laser group. The enhancement of PTT efficacy of DPN could attribute to the high accumulation in tumor, deep penetration in tumor tissue, and high production of thermal energy upon NIR irradiation.

3. Conclusion

The DPN was developed for deep tumor penetration and PTT of metastatic breast cancer. DPN was homogeneous nanometer-sized particles with the mean diameter within 20–30 nm. Upon 808 nm laser irradiation, DPN exhibited obviously enhanced temperature elevation over free DiR in metastatic 4T1 cells, thereby leading to the significant inhibition of cell proliferation and migration activity. In tumor bearing mice, the nanometer-sized DPN resulted in an obviously enhanced accumulation in tumor, and could penetrate into the deep interior of tumor tissues. Moreover, the combination of DPN with NIR laser irradiation produced significant elevation of tumor surface temperature, and could almost entirely inhibit the progression of primary tumor and lung metastasis of breast cancer. Therefore, DPN could provide a promising deep tumor-penetrating photothermal nanotherapeutics and improve therapeutic effect of tumor by the simultaneous inhibition of growth and metastasis of breast cancer.

4. Experimental Section

Materials: The methyl poly(ethylene glycol) (mPEG–OH, M_w 5000) was purchased from Beijing Jenkem Technology Co. Ltd (Beijing, China) and the 2-(diisopropylamino)ethyl methacrylate was obtained from Sinopharm chemical reagent Co. Ltd (Shanghai, China). The diblock copolymer of poly(ethylene glycol)-*block*-poly(2-diisopropyl methacrylate) (PEG-*b*-PDPA$_{10}$) was synthesized by the ATRP method.[32] The DiR was provided by Amyjet Scientific Inc. (Wuhan, China). D-luciferin was purchased from Perkin-Elmer (USA). Fetal bovine serum (FBS) and RPMI1640 cell culture media were supplied by Gibco Life Technologies. Other chemicals were of analytical grade.

Cells and Animals: The 4T1 cell line was obtained from Shanghai Cell Bank, Chinese Academy of Sciences (CAS), and 4T1-luc cells with stable expression of luciferase were provided by Keyuandi Biotech Co. Ltd. (Shanghai, China). Both kinds of cells were cultured in RPMI 1640 supplemented with 10% FBS, 100 U mL^{-1} penicillin G sodium, and 100 μg mL^{-1} streptomycin sulfate. Cells were maintained at 37 °C in an incubator with a humidified atmosphere and 5% CO_2 concentration. Female BALB/c nude mice (18–22 g) were purchased from Shanghai Laboratory Animal Center, CAS, and acclimatized under the animal care facility for 5 d prior to the animal experiments. The protocols were approved by the Institutional Animal Care and Use Committee (IACUC) of Shanghai Institute of Materia Medica, CAS.

Preparation and Characterization of DPN: The DPN was prepared by the solvent diffusion method. Briefly, DiR and PEG-*b*-PDPA$_{10}$ (1:100, w/w) were dissolved in methanol and diluted into 20 times of distilled water. Then, the mixed solution was dialyzed against water to remove the methanol to form DPN spontaneously, and the terminal concentration of DiR was 0.2 mg mL^{-1}. The morphology and particle size of DPN were determined by TEM (JEOL JEM-2100F, Japan). Samples were mounted onto the copper grid, negatively stained with phosphotungstic acid solution (1%, w/v) and then dried at room temperature for the measurements. The size distribution of DPN was further evaluated by image analysis. The fluorescence spectra of DiR in water and DPN were measured on a fluorescence spectrometer (F4600, HITACHI, Japan) with excitation at 745 nm. Then, the thermal profiles of DiR in water and DPN were determined with an infrared thermal camera (A150-15-M, Irtech Ltd.). Samples (containing 200 μg mL^{-1} of DiR) were irradiated with a 808 nm laser (MDL-N-10W, Changchun New Industries, China) at 2.5 W cm^{-2} for 5 min. The infrared thermographic images were recorded and the temperatures at different time points were analyzed by the accompanied software. By contrast, the distilled water was performed in the same procedure as negative control.

Photothermal Profiles and Cytotoxicity in 4T1 Cells: To determine the PTT ability of DPN on cell viability, the photothermal profiles of DPN in 4T1 breast cancer cells were evaluated in comparison with free DiR. Briefly, 4T1 cells were seeded in 24-well plates at a density of 5×10^4 per well and incubated overnight. Then, free DiR or DPN was added to the culture media at 0.1 mg mL^{-1} of DiR and incubated for further 4.0 h. Afterward, cells were replaced with fresh media and exposed to the 808 nm laser irradiation at a power density of 2.5 W cm^{-2}. Temperature changes were recorded with the infrared thermal camera for 3 min. Then, the photothermal cytotoxicity in 4T1 cells was analyzed by the LIVE/DEADViability/Cytotoxicity Kit (Life technologies). In brief, 4T1 cells were seeded in 96-well plates at 5×10^3 per well and cultured overnight. Then, the growth media were replaced with fresh media containing DiR or DPN at 0.1 mg mL^{-1} of DiR. After 4 h incubation, cells were rinsed with PBS and irradiated with the 808 nm laser at 2.5 W cm^{-2} for 5 min. By contrast, nontreated cells, cell treated with free DiR and DPN without NIR irradiation, and nontreated cells only exposed to 808 nm laser were performed as control. Then, cells were treated with LIVE/DEADViability/Cytotoxicity Kit according to the manufacturer's protocol and detected under a fluorescent microscope (IX81, Olympus, Japan).

In Vitro PTT Ability on Inhibition of Cell Migration: Transwell migration assay was utilized to evaluate the PTT effects of DPN on cell migration activities of metastatic 4T1 cells. Briefly, cells were seeded in 24-well plates at a density of 5×10^4 per well and allowed to attach for 12 h prior to photothermal treatment. After the media were replaced, DiR or DPN was added onto the cells and the terminal concentration of DiR was 0.1 mg mL^{-1}. Followed by 4 h incubation, the media were changed and cells were exposed to the 808 nm laser for only 1 min. To avoid the interference of photothermal cytotoxicity on cell migration, the cell viability after the NIR laser irradiation was assessed by the LIVE/DEADViability/Cytotoxicity Kit as described above. For the cell migration assay, the NIR irradiated cells were collected, rinsed, resuspended in 100 μL of serum-free media and then added to the upper chambers of transwells (24-well insert, pore size 8 μm, Costar, USA), while 600 μL of fresh culture media with 10% FBS was added to the lower chambers of 24-well culture plate. After 24 h, cells in the upper chambers were removed with a cotton swab. The migrated cells across the membrane were stained with crystal violet, photographed under a microscope and counted in three predetermined fields for quantification. By contrast, the cell migration assay of nontreated cells and cell treated with free DiR and DPN without NIR irradiation were performed as control.

In Vivo Imaging and Distribution in Tumor Tissues: The in vivo biodistribution of DPN in tumor bearing mice was investigated by NIR fluorescence imaging analysis. The metastatic breast cancer model was induced by 4T1-luc cell line, which was a lung metastatic cell line derived from a mammary tumor. A total of 5×10^5 4T1-luc cells were injected to the second right mammary fat pad of mice. When the tumor volume reached to 150–200 mm^3, free DiR and DPN were, respectively, administered to mice via tail injection at a dose of 40 μg DiR per mouse. At 0.5, 1, 2, 4, and 6 h after administration, mice were anesthetized and imaged under the in vivo imaging system (IVIS Spectrum, Perkin-Elmer). Typically at 1.0 h after injection, mice were sacrificed, and major organs including heart, liver, spleen, lung, kidney, and tumor carefully removed for visualization under the imaging system. The fluorescent signals of each organ were analyzed by the accompanied software. Moreover, the deep penetration of DPN in tumor tissue was further measured by photoacoustic imaging. At 1.0 h after intravenous administration of DPN, tumor was carefully removed, rinsed with PBS, and embedded in ultrasound gel for the measurements. Samples were scanned to the full extent of tumor by the MSOT imaging system (in Vision 128, iTheraMedical, Germany).

In Vivo Temperature Measurement During NIR Irradiation: The in vivo photothermal profiles in tumor xenograft model during NIR irradiation were determined with the infrared thermal imaging camera (A150-15-M, Irtech Ltd.). The tumor bearing mice was developed as described above. When the tumor volume reached 100–150 mm^3, free DiR and DPN were intravenously administered to mice at a dose of 40 μg DiR per mouse, respectively. By contrast, mice with NIR irradiation alone were performed as control. At 1.0 h after injection, mice were anesthetized and the tumors were exposed to the 808 nm laser at 2.5 W cm^{-2} for 5 min. The region maximum temperature and infrared thermographic images were obtained by the infrared thermal imaging camera.

In Vivo PTT on Progression and Lung Metastasis of Breast Cancer: The metastatic breast cancer model was induced by 4T1-luc cells as described above. At day 8 after the inoculation, mice were randomly divided into four groups of saline control, laser alone, free DiR+laser, and DPN+laser ($n = 6$). Free DiR and DPN were intravenously administered to mice at doses equivalent to 40 μg DiR per mouse. At 1.0 h after the injection, mice were exposed to 808 nm laser at 2.5 W cm^{-2} for 5 min. The treated animals were maintained in the animal care facility, and the tumor size and body weight were measured at predetermined time intervals. At the end point, mice were autopsied and lung tissues were removed to detect the lung metastasis. The lung tissues were rinsed with saline, and immersed in D-lucifer in solution (5 mg mL^{-1}, Perkin-Elmer) for 10 min. Afterward, the bioluminescence signals from these lung tissues were detected under the in vivo imaging system (IVIS Spectrum, Perkin-Elmer). Moreover, the histological examinations of lung tissues were performed by H&E staining to detect the metastatic foci in lungs.

Statistic Analysis: Data were presented as mean ± standard deviation (SD). Student's t-test was applied to test the significance of the difference, which was considered to be significant when $p < 0.05$ and very significant when $p < 0.01$.

Supporting Information

Supporting Information is available from the Wiley Online Library or from the author.

Acknowledgements

The National Basic Research Program of China (2015CB932103, 2013CB932503) and the National Natural Science Foundation of China (81270047, 81373359) are gratefully acknowledged for financial support.

Received: February 26, 2015
Published online: April 8, 2015

[1] B. L. Eckhardt, P. A. Francis, B. S. Parker, R. L. Anderson, *Nat. Rev. Drug Discovery* **2012**, *11*, 479.
[2] R. Siegel, D. Naishadham, A. Jemal, *CA Cancer J. Clin.* **2013**, *63*, 11.
[3] C. B. Matsen, L. A. Neumayer, *JAMA Surg.* **2013**, *148*, 971.

[4] R. Hatami, A. M. Sieuwerts, S. Izadmehr, Z. Yao, R. F. Qiao, L. Papa, M. P. Look, M. Smid, J. Ohlssen, A. C. Levine, D. Germain, D. Burstein, A. Kirschenbaum, A. DiFeo, J. A. Foekens, G. Narla, *Sci. Transl. Med.* **2013**, *5*, 169ra12.

[5] Y. Fernandez, J. Cueva, A. G. Palomo, M. Ramos, A. de Juan, L. Calvo, J. Garcia-Mata, P. Garcia-Teijido, I. Pelaez, L. Garcia-Estevez, *Cancer Treat. Rev.* **2010**, *36*, 33.

[6] A. Schroeder, D. A. Heller, M. M. Winslow, J. E. Dahlman, G. W. Pratt, R. Langer, T. Jacks, D. G. Anderson, *Nat. Rev. Cancer* **2012**, *12*, 39.

[7] a) V. Shanmugam, S. Selvakumar, C. S. Yeh, *Chem. Soc. Rev.* **2014**, *43*, 6254; b) A. M. Alkilany, L. B. Thompson, S. P. Boulos, P. N. Sisco, C. J. Murphy, *Adv. Drug Delivery Rev.* **2012**, *64*, 190.

[8] Z. Zhang, J. Wang, C. Chen, *Adv. Mater.* **2013**, *25*, 3869.

[9] S. H. Hu, R. H. Fang, Y. W. Chen, B. J. Liao, I. W. Chen, S. Y. Chen, *Adv. Funct. Mater.* **2014**, *24*, 4144.

[10] Y. Ma, X. Liang, S. Tong, G. Bao, Q. Ren, Z. Dai, *Adv. Funct. Mater.* **2013**, *23*, 815.

[11] a) X. Song, H. Gong, S. Yin, L. Cheng, C. Wang, Z. Li, Y. Li, X. Wang, G. Liu, Z. Liu, *Adv. Funct. Mater.* **2014**, *24*, 1194; b) Q. Tian, Q. Wang, K. X. Yao, B. Teng, J. Zhang, S. Yang, Y. Han, *Small* **2014**, *10*, 1063.

[12] J. Chen, M. Yang, Q. Zhang, E. C. Cho, C. M. Cobley, C. Kim, C. Glaus, L. V. Wang, M. J. Welch, Y. Xia, *Adv. Funct. Mater.* **2010**, *20*, 3684.

[13] a) X. Q. Huang, S. H. Tang, B. J. Liu, B. Ren, N. F. Zheng, *Adv. Mater.* **2011**, *23*, 3420; b) C. Li, T. Chen, I. Ocsoy, G. Zhu, E. Yasun, M. You, C. Wu, J. Zheng, E. Song, C. Z. Huang, W. Tan, *Adv. Funct. Mater.* **2014**, *24*, 1772; c) L. Zhang, S. Gao, F. Zhang, K. Yang, Q. Ma, L. Zhu, *ACS Nano* **2014**, *8*, 12250; d) T. Liu, C. Wang, X. Gu, H. Gong, L. Cheng, X. Shi, L. Feng, B. Sun, Z. Liu, *Adv. Mater.* **2014**, *26*, 3433.

[14] a) M. Guo, J. Huang, Y. Deng, H. Shen, Y. Ma, M. Zhang, A. Zhu, Y. Li, H. Hui, Y. Wang, X. Yang, Z. Zhang, H. Chen, *Adv. Funct. Mater.* **2015**, *25*, 59; b) J. Liu, C. Wang, X. Wang, X. Wang, L. Cheng, Y. Li, Z. Liu, *Adv. Funct. Mater.* **2015**, *25*, 384.

[15] a) S. Sharifi, S. Behzadi, S. Laurent, M. L. Forrest, P. Stroeve, M. Mahmoudi, *Chem. Soc. Rev.* **2012**, *41*, 2323; b) J. X. Li, X. L. Chang, X. X. Chen, Z. J. Gu, F. Zhao, Z. F. Chai, Y. L. Zhao, *Biotechnol. Adv.* **2014**, *32*, 727; c) S. M. Hussain, L. K. Braydich-Stolle, A. M. Schrand, R. C. Murdock, K. O. Yu, D. M. Mattie, J. J. Schlager, M. Terrones, *Adv. Mater.* **2009**, *21*, 1549.

[16] a) J. Zhou, Z. G. Lu, X. J. Zhu, X. J. Wang, Y. Liao, Z. F. Ma, F. Y. Li, *Biomaterials* **2013**, *34*, 9584; b) X. H. Zheng, D. Xing, F. F. Zhou, B. Y. Wu, W. R. Chen, *Mol. Pharm.* **2011**, *8*, 447; c) P. Huang, P. F. Rong, A. Jin, X. F. Yan, M. G. Zhang, J. Lin, H. Hu, Z. Wang, X. Y. Yue, W. W. Li, G. Niu, W. B. Zeng, W. Wang, K. C. Zhou, X. Y. Chen, *Adv. Mater.* **2014**, *26*, 6401; d) F. P. Gao, Y. X. Lin, L. L. Li, Y. Liu, U. Mayerhoffer, P. Spenst, J. G. Su, J. Y. Li, F. Wurthner, H. Wang, *Biomaterials* **2014**, *35*, 1004; e) M. B. Zheng, C. X. Yue, Y. F. Ma, P. Gong, P. F. Zhao, C. F. Zheng, Z. H. Sheng, P. F. Zhang, Z. H. Wang, L. T. Cai, *ACS Nano* **2013**, *7*, 2056; f) H. Gong, L. Cheng, J. Xiang, H. Xu, L. Feng, X. Shi, Z. Liu, *Adv. Funct. Mater.* **2013**, *23*, 6059; g) L. Cheng, W. He, H. Gong, C. Wang, Q. Chen, Z. Cheng, Z. Liu, *Adv. Funct. Mater.* **2013**, *23*, 5893.

[17] C. X. Yue, P. Liu, M. B. Zheng, P. F. Zhao, Y. Q. Wang, Y. F. Ma, L. T. Cai, *Biomaterials* **2013**, *34*, 6853.

[18] F. M. Youniss, G. Sundaresan, L. J. Graham, L. Wang, C. R. Berry, G. K. Dewkar, P. Jose, H. D. Bear, J. Zweit, *PLoS One* **2014**, *9*, e109162.

[19] H. Cho, G. L. Indig, J. Weichert, H. C. Shin, G. S. Kwon, *Nanomedicine* **2012**, *8*, 228.

[20] a) K. Park, S. Lee, E. Kang, K. Kim, K. Choi, I. C. Kwon, *Adv. Funct. Mater.* **2009**, *19*, 1553; b) J. J. Xu, W. W. Zhao, S. Song, C. Fan, H. Y. Chen, *Chem. Soc. Rev.* **2014**, *43*, 1601.

[21] a) M. Eisenblatter, J. Ehrchen, G. Varga, C. Sunderkotter, W. Heindel, J. Roth, C. Bremer, A. Wall, *J. Nucl. Med.* **2009**, *50*, 1676; b) J. Ruan, H. Song, C. Li, C. Bao, H. Fu, K. Wang, J. Ni, D. Cui, *Theranostics* **2012**, *2*, 618.

[22] L. Li, J. Sun, Z. He, *Curr. Med. Chem.* **2013**, *20*, 2881.

[23] I. F. Tannock, A. Primeau, R. Grantab, C. Lee, *J. Clin. Oncol.* **2005**, *23*, 852s.

[24] a) N. Bertrand, J. Wu, X. Xu, N. Kamaly, O. C. Farokhzad, *Adv. Drug Delivery Rev.* **2014**, *66*, 2; b) E. Vlashi, L. E. Kelderhouse, J. E. Sturgis, P. S. Low, *ACS Nano* **2013**, *7*, 8573.

[25] F. Danhier, O. Feron, V. Preat, *J. Controlled Release* **2010**, *148*, 135.

[26] R. Tong, H. H. Chiang, D. S. Kohane, *Proc. Natl. Acad. Sci. U.S.A.* **2013**, *110*, 19048.

[27] C. Y. Ju, R. Mo, J. W. Xue, L. Zhang, Z. K. Zhao, L. J. Xue, Q. N. Ping, C. Zhang, *Angew. Chem. Int. Ed.* **2014**, *53*, 6253.

[28] a) C. Wong, T. Stylianopoulos, J. A. Cui, J. Martin, V. P. Chauhan, W. Jiang, Z. Popovic, R. K. Jain, M. G. Bawendi, D. Fukumura, *Proc. Natl. Acad. Sci. U.S.A.* **2011**, *108*, 2426; b) K. Y. Huang, H. L. Ma, J. Liu, S. D. Huo, A. Kumar, T. Wei, X. Zhang, S. B. Jin, Y. L. Gan, P. C. Wang, S. T. He, X. N. Zhang, X. J. Liang, *ACS Nano* **2012**, *6*, 4483.

[29] H. Cabral, Y. Matsumoto, K. Mizuno, Q. Chen, M. Murakami, M. Kimura, Y. Terada, M. R. Kano, K. Miyazono, M. Uesaka, N. Nishiyama, K. Kataoka, *Nat. Nanotechnol.* **2011**, *6*, 815.

[30] Z. Zhang, H. Cao, S. Jiang, Z. Liu, X. He, H. Yu, Y. Li, *Small* **2014**, *10*, 4735.

[31] A. J. Minn, G. P. Gupta, P. M. Siegel, P. D. Bos, W. P. Shu, D. D. Giri, A. Viale, A. B. Olshen, W. L. Gerald, J. Massague, *Nature* **2005**, *436*, 518.

[32] H. Yu, Y. Zou, Y. Wang, X. Huang, G. Huang, B. D. Sumer, D. A. Boothman, J. Gao, *ACS Nano* **2011**, *5*, 9246.